JACS
JOURNAL OF THE AMERICAN CHEMICAL SOCIETY
Article
Cite This: J. Am. Chem. Soc. 2019, 141, 12545−12557
pubs.acs.org/JACS

A Multifunctional Cosolvent Pair Reveals Molecular Principles of Biomass Deconstruction

Abhishek S. Patri,[†,‡,§] Barmak Mostofian,[⊥,#] Yunqiao Pu,[§,∥,#] Nicholas Ciaffone,[▽] Mikhael Soliman,[▽] Micholas Dean Smith,[⊥,□] Rajeev Kumar,[‡,§,∥] Xiaolin Cheng,[⊥,◆] Charles E. Wyman,[†,‡,§,∥] Laurene Tetard,[▽,¶] Arthur J. Ragauskas,[§,∥,#,●] Jeremy C. Smith,[⊥,□] Loukas Petridis,[⊥,□] and Charles M. Cai*[,†,‡,§,∥]

[†]Department of Chemical and Environmental Engineering, Bourns College of Engineering, University of California, Riverside, 900 University Avenue, Riverside, California 92521, United States

[‡]Center for Environmental Research and Technology, Bourns College of Engineering, University of California, Riverside, 1084 Columbia Avenue, Riverside, California 92507, United States

[§]BioEnergy Science Center (BESC), and [∥]Center for Bioenergy Innovation (CBI), Oak Ridge National Laboratory (ORNL), Oak Ridge, Tennessee 37831, United States

[⊥]UT/ORNL Center for Molecular Biophysics, and [#]Joint Institute for Biological Sciences, Oak Ridge National Laboratory, Oak Ridge, Tennessee 37830, United States

[▽]NanoScience Technology Center and [¶]Department of Physics, University of Central Florida, Orlando, Florida 32826, United States

[□]Department of Biochemistry & Cellular Molecular Biology, and [●]Department of Chemical and Biomolecular Engineering, The University of Tennessee, Knoxville, Tennessee 37996, United States

[◆]College of Pharmacy, The Ohio State University, Columbus, Ohio 43210, United States

Supporting Information

ABSTRACT: The complex structure of plant cell walls resists chemical or biological degradation, challenging the breakdown of lignocellulosic biomass into renewable chemical precursors that could form the basis of future production of green chemicals and transportation fuels. Here, experimental and computational results reveal that the effect of the tetrahydrofuran (THF)−water cosolvents on the structure of lignin and on its interactions with cellulose in the cell wall drives multiple synergistic mechanisms leading to the efficient breakdown and fractionation of biomass into valuable chemical precursors. Molecular simulations show that THF−water is an excellent "theta" solvent, such that lignin dissociates from itself and from cellulose and expands to form a random coil. The expansion of the lignin molecules exposes interunit linkages, rendering them more susceptible to depolymerization by acid-catalyzed cleavage of aryl-ether bonds. Nanoscale infrared sensors confirm cosolvent-mediated molecular rearrangement of lignin in the cell wall of micrometer-thick hardwood slices and track the disappearance of lignin. At bulk scale, adding dilute acid to the cosolvent mixture liberates the majority of the hemicellulose and lignin from biomass, allowing unfettered access of cellulolytic enzymes to the remaining cellulose-rich material, allowing them to sustain high rates of hydrolysis to glucose without enzyme deactivation. Through this multiscale analysis, synergistic mechanisms for biomass deconstruction are identified, portending a paradigm shift toward first-principles design and evaluation of other cosolvent methods to realize low cost fuels and bioproducts.

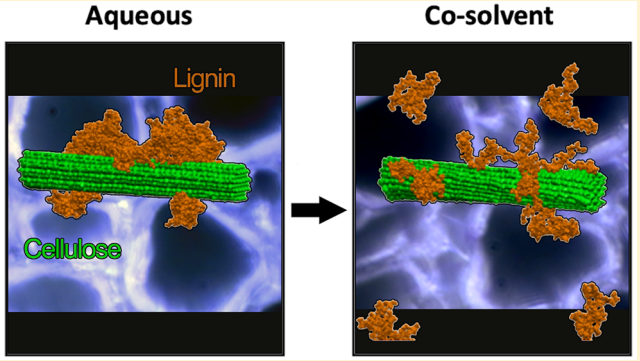

INTRODUCTION

One of the greatest scientific and engineering challenges of our time is to provide pathways for modern chemical and fuel industries to transition to a fully sustainable practice of utilizing renewable resources.[1−4] Lignocellulosic biomass is the most abundant source of organic carbon on Earth and is the only suitable feedstock capable of supporting renewable energy production in a developing bioeconomy at scales relevant to positively impacting global warming.[5−10] However, plant biomass has evolved to form complex structures that resist breakdown to precursors amenable to conversion into valuable

Received: September 21, 2018
Published: July 15, 2019

DOI: 10.1021/jacs.8b10242
J. Am. Chem. Soc. 2019, 141, 12545−12557

chemicals. Lignin in biomass serves as both a shield to block chemical and biological access to sugars as well as an inhibitor of cellulolytic (cellulase) enzymes.[11−15] Moreover, cellulose is tightly packed in microfibrils that exhibit high crystallinity and degree of polymerization, contributing to its recalcitrance.[16] Additionally, xylan oligomers and other polysaccharides from hemicellulose also cause severe cellulase inhibition in cellulose conversion to sugars.[17,18]

Methods for biomass deconstruction have traditionally focused on improving recovery of monomeric sugars from biomass. Aqueous methods, such as hydrothermal and dilute acid pretreatments, have been developed to reduce limiting factors, such as cellulose degree of polymerization and enzyme inhibition by hemicellulose sugars, thus achieving modest improvements in sugar yields upon enzymatic digestion while largely ignoring lignin.[19−21] Lignin removal from the cell wall and subsequent processing is challenging due to its chemical structure and resistance to chemical and biological manipulation in aqueous environments. Lignin is also more chemically diverse and energy dense than cellulose, and its potential value as a primary feedstock for conversion to renewable chemicals, materials, and fuels has long been recognized.[22−25] However, limited understanding of lignin−solvent−cellulose interactions has prevented the effective selection and utilization of organic solvents to augment both sugar recovery and lignin utilization simultaneously.

As a result, recent focus has emphasized disparate approaches to achieving either high yields from polysaccharide hydrolysis or targeted extraction and depolymerization of residual lignin toward value-added products.[19,26−28] For example, ammonia fiber expansion (AFEX)[29] reduces cellulose recalcitrance by cleaving lignin−carbohydrate complex linkages[30] and alcohol or ketone organosolv[31−36] pretreatment dissolves lignin from biomass at very severe reaction conditions in order to achieve high cellulose digestibility, often compromising total sugar yields. However, drawbacks such as costly process economics,[37] reduced overall sugar yields due to severe degradation of hemicellulose sugars, and low ethanol yields during high-solid fermentations have hampered commercial adoption of these methods.[31−35,38] Meanwhile, sulfite and ionic liquid pretreatments have made strides toward increasing enzymatic sugar yields and improving ethanol titers achieved from biomass feedstocks, albeit still requiring significant enzyme loadings.[39−42] Such pretreatment methods, however, have yet to demonstrate total carbon utilization from lignocellulosic feedstocks by integrating the production of fermentable sugars with the generation of value-added products derived from lignin. Moving forward, it is critical for efficient and green techniques to be developed whereby high yields of biomass polymers suitable for subsequent valorization can be achieved.[7,8] Key to this is maximizing total utilization of carbon by simultaneously enhancing both the efficient hydrolysis of polysaccharides and the extraction and depolymerization of lignin.[43]

To address this, new biomass pretreatment methods employing multifunctional cosolvents have emerged. Tetrahydrofuran (THF) and γ-valerolactone (GVL) are cosolvents to water that have demonstrated unique molecular level functionalities to promoting both biomass solubilization and lignin fractionation beyond other cosolvents and organosolv methods.[44−46] The use of the THF cosolvent, in particular, has made significant strides in demonstrating improved biomass deconstruction and delignification performance. Specifically, the biomass pretreatment process that applies THF−water cosolvents with dilute acid at temperatures between 140 and 200 °C is called the "Cosolvent Enhanced Lignocellulosic Fractionation" (CELF) process. Previous experimental studies have reported that both woody and agricultural biomass materials prepared by CELF, employing THF cosolvent concentrations as low as 50%, can be subsequently hydrolyzed by cellulolytic enzymes to recover more than 90% of the total available sugars into a concentrated water solution. Surprisingly, the high sugar recovery was accomplished with an order of magnitude less of enzyme required than for aqueous dilute acid pretreated materials and supported high solids simultaneous saccharification and fermentation (SSF) to achieve more than 85 g/L ethanol titers.[45−49] Products and substrates produced by CELF pretreatment of biomass have been integrated with both heterogeneous catalytic methods and advanced fermentation methods to achieve higher fuel yields supporting improved process economics for second generation biofuel production than what was possible with conventional aqueous processes.[50−52] A comprehensive understanding of the molecular principles behind the effectiveness of the THF−water cosolvent pair would facilitate the identification of other highly functional cosolvents to support a more rational design of integrative biomass deconstruction methods in the future. However, a combined set of molecular principles governing enhanced biomass deconstruction by cosolvent interactions with biomass remain largely unexplored.

Here, we focus on understanding, across multiple scales, the physical and chemical changes that occur in the cell wall components lignin, cellulose, and hemicellulose, as they are exposed to the THF−water cosolvent during thermochemical pretreatment in nonacid and dilute acid conditions. Previous work has indicated that this cosolvent pair is unique among aqueous−organic solvent systems in that it not only functions well for high solid loadings, but it also has been found to preferentially solvate lignin, modulate hemicellulose conversion, and undergo a phase separation at cellulose surfaces.[53−57] In this study, we demonstrate how this cosolvent combination promotes lignin release from cellulose, enhances lignin depolymerization, and improves enzyme reactivity to cellulose, which together lead to the enhancement of biomass deconstruction. Key to this work is that the methodology used here may further be applicable to the evaluation of other promising cosolvents, which will begin the communal shift toward the rational design of "lignin-first" biomass deconstruction techniques.

EXPERIMENTAL SECTION

Molecular Dynamics (MD) Simulations. A lignocellulose structure was simulated in an equivolume mixture of THF−water and in pure water. The cellulose Iβ fiber consisted of 36 chains, each containing 40 glucose monomers (DP40),[58] and 10 branched lignin molecules, each consisting of 61 guaiacyl (G) monomers. The lignin monomer type, linkage composition, and branching distribution correspond to that of softwood lignin, as described elsewhere.[59] The initial coordinates of the cellulose and lignin were taken from the end of a previous simulation performed in water, during which lignin molecules collapsed and aggregated predominantly onto the hydrophobic surfaces of the cellulose fiber (structure on the left of Figure 1). Both the cellulose:lignin weight ratio (∼2:1) and the solid loading (∼5 wt %) roughly correspond to the experiments. The total number of atoms in a simulation system was greater than 1.5 million. We focused on lignin and cellulose because their interaction contributes considerably to the recalcitrance of pretreated biomass.[60] Although

DOI: 10.1021/jacs.8b10242
J. Am. Chem. Soc. 2019, 141, 12545−12557

solubilization of hemicellulose is important when deconstructing biomass, it was not examined here because it is not affected significantly by THF as xylans are readily removed from biomass using dilute acid, both in the presence of THF and without THF.[49] The breakdown of the hemicellulose−-lignin matrix, which may affect the overall biomass solubility, was thus not considered in the simulation, but the impact of hemicellulose removal toward cellulose digestibility is revealed by the enzymatic experiments in this study. The aim of the calculations is not to construct a full plant cell wall model and to simulate the entirety of biomass pretreatment, which is currently impossible. The models investigate the lignin−cellulose interaction because it is a major contributor to the recalcitrance of pretreated biomass[60] and because other polysaccharides are mostly removed from biomass using dilute acid, both in the presence of THF and without THF.

The CHARMM[61−64] force field parameters and the TIP3P[65] water model were used. After energy minimization and equilibration in the NPT ensemble at T = 445 K and ambient pressure, MD simulations were run with a time step of 2 fs. Three simulations of lignocellulose in the cosolvent mixture were run for 50 ns. All simulations were performed and analyzed with the GROMACS software version 5.0.1[66] on the TITAN supercomputer located at the Oak Ridge Leadership Computing Facility (OLCF). Visualization and rendering of molecular images was performed using the VMD software.[67]

We also simulated eight initially disassociated lignin decamers (lignin polymers with DP10 and the same linkage composition as above), in the absence of cellulose, in water for 100 ns until stable aggregates were formed. THF then was added to the simulation to obtain a 1:1 v/v THF−water cosolvent environment, and the simulations were extended for an additional 50 ns.

Intermolecular atomic contacts are defined as the number of atoms that are less than 3.5 Å. The solvent-accessible surface area (SASA) of the lignin β-O-4 linkages is determined by a rolling probe of radius 1.4 Å. We note that MD simulations do not model chemical reactions, and all intermolecular interactions considered here are noncovalent, such as van der Waals and Coulomb.

Biomass Pretreatment. *Acer* (maple wood) reactions were carried out using air-dried *Acer* chips obtained in New York State by Mascoma Corp. (now Lallemand Inc., Lebanon, NH). *Populus* reactions were carried out using air-dried *Populus* chips provided by the National Renewable Energy Laboratory (NREL). Chips were knife milled to below 1 mm particle size in a model 4 Wiley Mill (Thomas Scientific, Swedesboro, NJ) at the University of California, Riverside. Consistent with the MD simulations and reactions with the knife-milled samples, the bulk-scale cosolvent reactions used a 1:1 volumetric mixture of THF (>99% purity, Fisher Scientific, Pittsburgh, PA) and deionized water. Concentrated sulfuric acid (72 wt %, Ricca Chemical Co.) was diluted in solution to obtain a final acid concentration of 0.05 M or 0.5 wt % in liquids to execute the dilute acid and CELF reactions. The bulk-scale pretreatment reactions were performed at 10 wt % solids loading in a 1 L Hastelloy Parr autoclave reactor (236HC Series, Parr Instruments Co., Des Moines, IL) equipped with a double-stacked pitch blade impeller operating at 200 rpm at reaction temperature of 160 °C for 25 min. The reactor temperature was measured directly using an in-line thermocouple (Omega, K-type). Pretreatment reaction temperatures were maintained by convective heating using a 4 kW fluidized sand bath (Techne, Princeton, NJ). To terminate the reaction, the reactor was cooled by being submerged into a large water bath at room temperature. Following pretreatment, pretreated solids were vacuum filtered and washed with deionized water until the pH of filtrate was greater than 5. The solids yield and moisture content were determined gravimetrically. Postpretreatment liquor was neutralized with 30% ammonium hydroxide until a pH of 7 was achieved. The liquor was then placed in a water bath set to 70 °C to boil off THF, causing the dissolved lignin fragments to precipitate. The precipitated lignin was then collected by vacuum filtration and washed with deionized water followed by washing with diethyl ether and then placed to dry for 12 h in an oven set to 40 °C.

Sodium Chlorite Delignification (Lignin Removal). Chlorite delignification was carried out inside a fume hood at 70 °C for 8 h in a water bath (StableTemp, Cole-Parmer, Vernon Hills, IL) by mixing 5 g of dry biomass in triplicate with 160 mL of deionized water followed by 3 g of sodium chlorite and 3 mL of acetic acid in a 500 mL Erlenmeyer flask (Fischer Scientific, Pittsburgh, PA).[68] The contents were thoroughly mixed by shaking the flasks, and a 50 mL Erlenmeyer flask was inverted in the mouth of the reaction flask to contain the reaction contents. Fresh additions of sodium chlorite and acetic acid were added every 2 h. Following completion of the reaction, the delignified solids were vacuum filtered and washed with room temperature deionized water until the pH of filtrate was above 5. Similar to pretreatment as discussed above, the total solids yield was determined gravimetrically.

Enzymatic Hydrolysis. As per the NREL protocol for Enzymatic Saccharification of Lignocellulosic Biomass,[69] enzymatic hydrolysis was performed in triplicate on samples prepared by CELF, aqueous dilute sulfuric acid pretreatment, and sodium chlorite bleaching. Avicel was not used in this study as it is a highly processed form of crystalline cellulose that may not accurately represent the features of biomass for rate studies. Enzymatic hydrolysis was performed in 125 mL Erlenmeyer flasks whereby 0.5 g of each biomass sample was added to a buffered water solution with a total working mass of 50 g (1 wt % solids loading). The water in the flasks also contained 50 mM citrate buffer (pH 4.9) to maintain hydrolysis pH and 0.02% sodium azide to prevent microbial contamination. Cellulase enzyme cocktail Accellerase 1500 with BCA protein content of 85 mg/mL (DuPont Industrial Biosciences, Palo Alto, CA) was delivered to the flasks to initiate cellulose hydrolysis and were based on total enzyme loadings of either 5 or 15 mg protein/g glucan in solids. Because the enzyme employed is primarily a cellulase, glucan conversion was determined by the concentration of glucose in the liquid measured at each time point. The flasks were incubated in a Multitron orbital shaker (Infors HT, Laurel, MD) set at 150 rpm and 50 °C and were preheated for an hour to reach uniform temperature before enzymes were inoculated. Samples of approximately 500 μL were centrifuged at 15 000 rpm for 10 min before being analyzed for glucose concentration by HPLC (high performance liquid chromatography) as described by a previous study.[70]

Quantification of Free Protein Content in Enzymatic Hydrolysis Liquid. A $NaBH_4$-based modified Ninhydrin assay was used to quantify total protein in enzymatic hydrolysis liquor with reduced interference from solubilized sugars.[71] One hundred microliters of sample or standard was incubated with 50 μL of 6.7 g/L $NaBH_4$ in a 1.5 mL microcentrifuge tube. Bovine serum albumin (BSA) in the range of 0−2000 mg/L was utilized as a protein standard. This was followed by the addition of 300 μL of 9 M HCl and subsequent heating in a dry oven at 130 °C for 2 h. After being cooled to room temperature, 100 μL of the sample was transferred to a fresh 1.5 mL microcentrifuge tube and neutralized with 100 μL of 5 M NaOH. Upon neutralization, 200 μL of 2% Ninhydrin reagent (Sigma-Aldrich Corp., St. Louis, MO) was added and heated at 100 °C for 10 min in a dry oven. After the mixture was cooled to room temperature, 500 μL of 50% (v/v) ethanol was added. Finally, 200 μL of colored solution was transferred to a 96-well microplate, and absorbance was read at 560 nm using a SpectraMax M2e Microplate Reader (Molecular Devices, Sunnyvale, CA). All samples were performed in triplicate.

Fractal Kinetics Modeling of Enzymatic Hydrolysis Rates. Fractal kinetic rates for glucan conversion during enzymatic hydrolysis were calculated on the basis of a first-order model, shown by eq 1. The fractal rate model correlates the conversion of glucan from only the cellulose in the substrate (C) to the enzyme incubation time. A total rate coefficient (k_t) is defined as a linear dependence between a rate constant, k, and time, t, raised to the fractal exponent, h. The details of the model setup and derivation are described in a previous study:[72]

$$\frac{dC}{dt} = k_t C, \text{ where } k_t = kt^h \quad (1)$$

DOI: 10.1021/jacs.8b10242
J. Am. Chem. Soc. 2019, 141, 12545−12557

Nonlinear regression package within MATLAB 7.0 (damped least-squares) was used to fit the experimental data from enzymatic hydrolysis at each time point to the model described in eq 2, in which X is glucan conversion (%) and t is time in hours:

$$X = 100^{*}\left\{1 - \exp\left[-k\left(1 + \frac{t^{1-h} - 1}{1 - h}\right)\right]\right\} \quad (2)$$

Raman, AFM, and NanoIR Imaging and Material Preparation. Cross sections of untreated *Populus* (obtained from ORNL green house) were prepared by microtome. The sections were subjected to treatment in an equivolume mixture of THF−water. The reactor was heated at T = 160 °C for 15, 30, and 60 min. All cross sections were characterized using Raman confocal spectroscopy (WITec Alpha300RA), while the cross sections treated for 30 min were studied with nanoscale infrared imaging (nanoIR2, Anasys Instruments).

Raman spectra were acquired using a 20× objective with 532 nm laser excitation and a 600 g/mm grating. Laser power and integration time were optimized to maintain the plant cell wall intact. AFM and nanoIR images were acquired with an Au-coated cantilever (PR-EX-nIR2, $k \approx 0.07-0.4$ N/m) in contact mode imaging. NanoIR measurements were carried out as described in ref 73. The laser pulse was tuned to match one of the cantilever resonances. At selected points, the wavelength of the laser was swept from 1530 to 1800 cm^{-1} with a 2 cm^{-1} step. At each wavelength, the frequency and intensity of the cantilever contact resonance were recorded to form an "absorption versus wavenumber" spectrum.

Analytical Methods on Raw Biomass. Compositional analysis of raw and pretreated *Acer* and *Populus* was conducted according to the established NREL procedure (version 8-30-2010) in triplicate.[74] All chemical analyses performed were based on Laboratory Analytical Procedures (LAPs) documented by NREL (Golden, CO). Liquid samples and appropriate calibration standards were analyzed using a high performance liquid chromatography (Agilent 1200) system equipped with a Bio-Rad Aminex HPX-87H column and refractive index (RI) detector) with a 5 mM sulfuric acid eluent at a flow rate of 0.6 mL/min. HPLC chromatograms were integrated using the Agilent Chemstation software package.

Lignin HSQC and ^{13}C NMR Analysis. Two-dimensional ^{13}C−^{1}H HSQC NMR experiments of control and recovered lignin samples were carried out in a Bruker Avance 400-MHz spectrometer operating at a frequency of 100.59 MHz for ^{13}C.[75,76] Quantitative ^{13}C NMR spectrum was acquired using deuterated dimethyl sulfoxide as solvent for lignin with a 90° pulse. An inverse-gated decoupling pulse sequence was used to avoid the nuclear Overhauser effect, and 10 240 scans were collected. A standard Bruker heteronuclear single quantum coherence (HSQC) pulse sequence (hsqcetgpspsi2) was used on a BBFO probe for HSQC analysis with deuterated dimethyl sulfoxide (DMSO-d_6) as solvent. The spectra were acquired with the following conditions: 13 ppm spectra width in F2 (^{1}H) dimension (1024 data points) and 210 ppm spectra width in F1 (^{13}C) dimension (256 data points), a 1.5 s pulse delay, a 90° pulse, and a $^{1}J_{C-H}$ of 145 Hz. The DMSO solvent peak (δ_C 39.5 ppm; δ_H 2.5 ppm) was used for chemical shifts calibration. Relative lignin interunit linkage abundance and monomer compositions were semiquantitatively calculated by using volume integration of contours in HSQC spectra.[77] NMR data and spectra processing was performed using TopSpin 2.1 software (Bruker BioSpin) and Adobe Illustrator CC (Adobe Inc.).

Lignin ^{31}P NMR Analysis. Quantitative ^{31}P NMR experiments were conducted on a Bruker Avance 400-MHz spectrometer. Lignin samples (~15 mg) were dissolved in a solvent mixture of pyridine and deuterated chloroform (1.6/1.0, v/v, 0.50 mL). The lignin sample was then derivatized with 2-chloro-4,4,5,5-tetramethyl-1,3,2-dioxaphospholane (TMDP). TMDP reacts with hydroxyl groups in lignin arising from aliphatic, phenolic, and carboxylic acids groups in the presence of pyridine to give phosphitylated products. The phosphitylated hydroxyls were then quantitatively measured using an internal standard that demonstrates satisfactory resolution from lignin hydroxyl regions in a ^{31}P NMR spectrum.[78] Chromium acetylacetonate and endo-*N*-hydroxy-5-norbornene-2,3-dicarboximide (NHND) were also added into the solution as relaxation agent and an internal standard, respectively. The spectrum was acquired using an inverse-gated decoupling pulse sequence (Waltz-16), 90° pulse, 25-s pulse delay, and 128−256 scans. All of the NMR data were processed using the TopSpin 2.1 software (Bruker BioSpin).

Lignin Molecular Weight Analysis. The lignin molecular weight analysis was performed with gel permeation chromatography (GPC) after acetylation.[75] The dry lignin samples were dissolved in a mixture of acetic anhydride/pyridine (1:1, v/v) and stirred at room temperature for 24 h. The solvents were removed by rotoevaporation at 45 °C with ethanol. The addition and removal of ethanol was repeated until a trace of acetic acid was removed from the samples. The acetylated lignin samples were dried under vacuum at 45 °C overnight prior to GPC analysis. The molecular weight distributions of the acetylated lignin samples were analyzed on a PSS-Polymer Standards Service (Warwick, RI) GPC SECurity 1200 system featuring Agilent HPLC 1200 components equipped with four Waters Styragel columns (HR1, HR2, HR4, and HR6) and a UV detector (270 nm). THF was used as the mobile phase with the flow rate of 1.0 mL/min. Polystyrene narrow standards were used for establishing the calibration curve. Data collection and processing were performed using Polymer Standards Service WinGPC Unity software (Build 6807), and molecular weights were calculated by the software relative to the polystyrene calibration curve.

RESULTS

Molecular Dynamics Predicts Lignin Dissociation from Cellulose in a Cosolvent Environment. To probe the molecular-level interactions between lignin and cellulose, we performed atomistic MD simulations of a lignocellulose structure, with lignin molecules initially bound noncovalently to the surface of a cellulose fiber, in pure water and in an equivolume THF−water cosolvent environment at 445 K (Figure 1 and movie S1). The purpose of the calculations is not to fully simulate the pretreatment of native biomass, but to probe how the conformations and interactions of cellulose and lignin are affected by the presence of THF in water. The simulations reveal two striking differences in the physical behavior of solutes in the two solvent environments (Figure 1A). First, the lignin molecules in THF−water dissociate from the cellulose and from each other, as indicated by the substantial decrease in the lignin−cellulose and lignin−lignin atomic contacts (Figure 1B,C) and the increase in the average interlignin distance (Figure S1A). THF is also found to disaggregate and dissolve the lignin molecules of lower molecular weight (DP10, Figure 1F). Second, solvation of lignin molecules in THF−water alters its conformation from compact globules (as typically adopted in water) to extended random coil conformations, as shown by the increase in their average radii of gyration (Figure 1D).

The underlying driving force behind both changes is that the interactions between lignin and the cosolvent are approximately equal in strength to the lignin−lignin interactions.[79] This makes THF−water a "theta" solvent for lignin.[54] In contrast, lignin−water interactions are less favorable than lignin−lignin interactions, making water a poor solvent for lignin and causing lignin to more likely associate with other lignin molecules and cellulose fibers.[58,80] Additionally, the observed association of THF with the hydrophobic faces of the cellulose strands will prevent lignin aggregation on those faces.[52]

The extended macromolecular configurations adopted by lignin in THF−water suggest greater potential reactivity for ether linkages (β-O-4) due to greater solvent-accessible surface

DOI: 10.1021/jacs.8b10242
J. Am. Chem. Soc. 2019, 141, 12545−12557

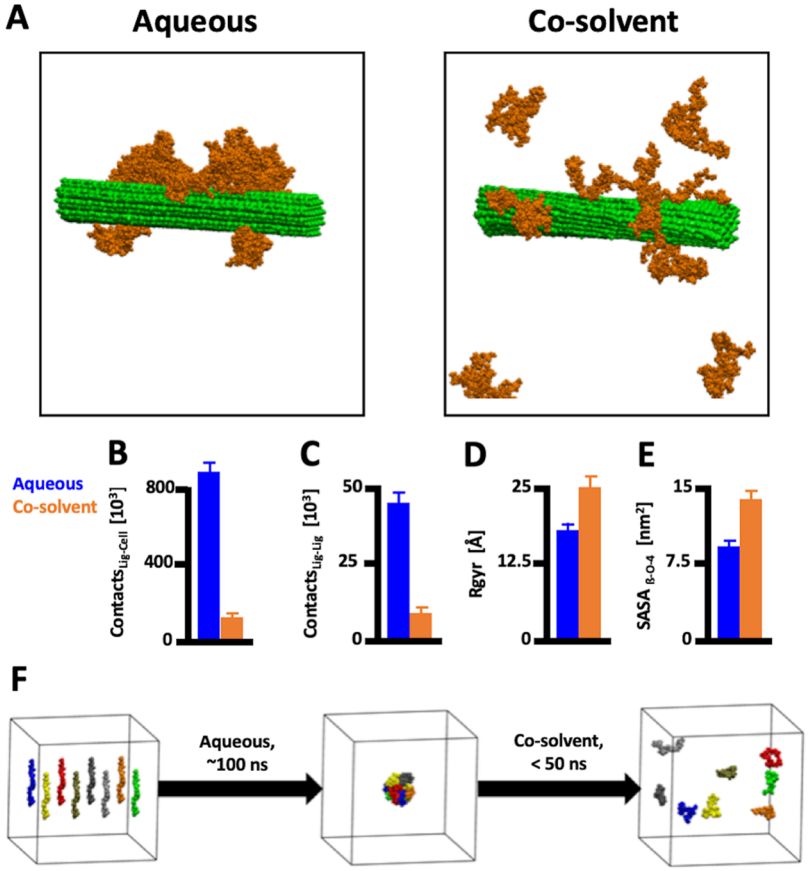

Figure 1. (A) MD simulation of lignocellulose in aqueous solution (left) and cosolvent mixture (right) after ∼50 ns. The cellulose fiber is shown in green and the lignin molecules in brown. In the cosolvent environment, almost all lignin molecules have dissociated from the cellulose fiber and from each other, changing their structure from compact (globular) to extended (coil) states. (B) Average lignin−cellulose, (C) lignin−lignin contact numbers, (D) lignin radius of gyration, and (E) solvent-accessible surface area of all β-O-4 lignin linkage atoms in the aqueous (blue) and in the cosolvent mixture (orange). The time-dependence of the number of contacts is shown in Figure S1B. (F) (Left) Starting structure of lignin simulation in water with different lignin decamers shown in different colors (average end-to-end distance d_e = 6.2 nm). (Middle) Within ∼100 ns, all lignin polymers have collapsed to a spherical aggregate binding noncovalently to each other (d_e = 2.2 nm). (Right) Upon addition of the cosolvent, the aggregate dissolves to individual lignin molecules (d_e = 3.4 nm) in less than 50 ns (movie S1).

area (SASA; Figure 1E). Further, by solvating the lignin and stacking on the hydrophobic surface of cellulose, the THF molecules displace water and localize the water molecules toward the ether bonds of both lignin and cellulose, where acid-catalyzed fragmentation or hydrolysis occurs. We propose that certain condensation (repolymerization) of lignin fragments is limited in the cosolvent environment, which constitutes an impediment to subsequent lignin valorization due to the entropic stabilization of the reactants.[52,54,81] In THF−water, the reactants (lignin fragments) are soluble and thus experience loss of entropy if they are covalently bonded due to condensation as the volume available for each fragment to explore is effectively decreased. Thus, condensation of the fragments is discouraged because the entropy of condensed products is smaller (less favorable) than that of the reactants. This difference in entropy between reactant and product is absent in aqueous solution, in which lignin fragments are aggregated irrespective of whether or not they are covalently bonded. In summary, the simulations performed strongly indicate that the presence of the THF cosolvent leads to lignin disaggregation, allowing the molecules to separate from the solid cellulose fraction and from each other while exposing lignin linkages to the solvent environment.

Raman and NanoIR Spectra Track Lignin Rearrangement in Biomass. Both the rearrangement of the lignin structure and the enhanced chemical accessibility of the lignin linkages observed by the MD simulations were experimentally validated by combined characterization by Raman, laser-induced fluorescence (LIF), and nanoIR of thin cross sections of hardwood *Populus* after treatment at 160 °C in an equivolume cosolvent mixture of THF−water, exposing the cell walls. First, Raman spectra were collected in multiple regions of the solids remaining after cosolvent treatment for different time durations (Figure 2). The decomposition, saccharification, and fermentation of biomass have previously been studied with Raman spectroscopy.[82−91] Raman spectroscopy provides a nondestructive and label-free approach to probe the content of plant cell walls. Changes in composition of the layers, including the orientation of lignin[90] or the crystallinity of cellulose,[84] can be detected using the distinct fingerprints of lignin and cellulose, respectively.[83] Although the interpretation of the complex Raman signature of plant cell walls can be challenging, foundational work by Agarwal et al.[84,89,91] and Gierlinger et al.[85−87] makes it possible to identify key structures in the plant composition using the bands corresponding to the aromatic functional group in lignin at ∼1600 cm^{-1} and to the carbohydrate group around 1100 cm^{-1}.

DOI: 10.1021/jacs.8b10242
J. Am. Chem. Soc. 2019, 141, 12545−12557

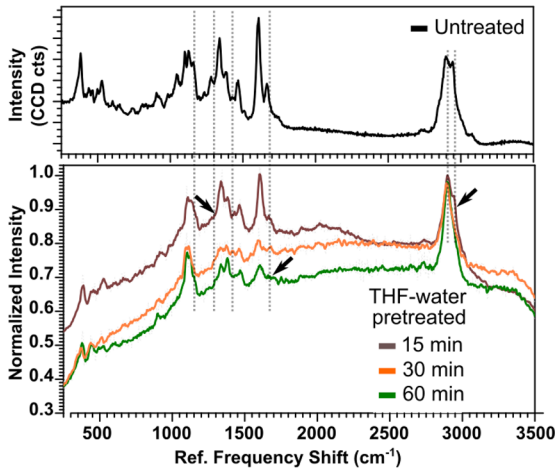

Figure 2. Microscale chemical analysis of the cell walls of untreated sample (black), and sample treated in THF−water cosolvent environment for 15 min (brown), 30 min (orange), and 60 min (green) by Raman spectroscopy. The dotted lines indicate changes summarized in Table S1.

Furthermore, advanced data processing algorithms have been developed to pinpoint multiparametric variations and their origins in the data sets.[92] However, the characterization of wood using Raman spectroscopy can be challenging due to the strong fluorescence signal resulting from lignin absorption in the visible.

Here, we find that morphological changes revealed by optical microscopy (Figure S4) are accompanied by a significant increase in laser-induced fluorescence (LIF)[93,94] (Figure S3). LIF[93,94] was observed after 15 min of treatment (Figure S3). Lahdetie et al.[93] demonstrated that the flexibility of the 5−5′ bond in lignin is responsible for LIF. In its untreated form (Figure 2), the fluorescence background of the Raman spectrum of poplar was sufficiently low for Raman active bands of cellulose, hemicellulose, and lignin to be clearly observed. This is likely due to the confinement of the lignin polymer in the complex polymeric matrix. LIF was found to increase as the lignin is released from the carbohydrate matrix of the cell wall. Longer treatments led to the decrease in LIF, which could be due to the loss of flexibility of the lignin upon aggregation.

After normalizing the data (Figure 2), we noted an overall decrease in the intensity of the bands corresponding to the C−H bond of the methoxyl group of lignin (2945 cm^{-1}) and to the aryl−OH linkage of lignin (1280 cm^{-1}), accompanied by a small shift in the stretching bond of the aryl band (1600 cm^{-1}). The intensity of the bands representing stretching in the ring conjugated C═C bond of lignin coniferyl alcohol (1660 cm^{-1}) and coniferaldehyde (1620 cm^{-1}) also decreased over the course of the reaction with THF−water at 160 °C. In contrast, cellulose bands around 1380 and 1150 cm^{-1} and a carbohydrate band around 2895 cm^{-1} remained, although we observed a small shift from 2900 to 2895 cm^{-1}. A more complete band assignment is provided in Table S1. Despite the rich information obtained with Raman spectroscopy, the spatial resolution of the information is limited by diffraction limit.

Considering this limitation, nanoscale chemical images of the untreated cross sections were obtained with nanoIR to better understand the distribution of the local chemical changes in the plant cell wall cross sections (Figure 3A−C). The fingerprints obtained after THF−water treatment (Figure 3H) were compared to those obtained on the nontreated cells (Figure 3G). NanoIR has previously been reported to achieve sub-100 nm lateral resolution.[95] The nanoIR spectra at different locations across the untreated cross section exhibited bands corresponding to the C═O and C═C vibrations (Figure 3G,H). The ratio of the band intensity of the C═O stretching in hemicellulose (ester)[96,97] at 1740 cm^{-1} and the aryl stretching in lignin at 1595 cm^{-1}[96,97] indicate significant changes with value of 1.3−1.5 in the secondary layers (points 1,2,3,5 in Figure 3B, G) and 0.8 in the middle lamella (point 4 in Figure 3B, G). Clear structural (Figure 3A and D) and chemical (Figure 3G,H and Figure S6) differences can be noted after the cosolvent reaction across the deconstructed cell walls. The data collected at various locations of poplar sections indicate a large heterogeneity of the residues remaining after treatment (Figure 3E,F). The IR spectra obtained on the cosolvent reacted tissues reveal the presence of a very strong aromatic band at ∼1595−1610 cm^{-1}, corresponding to modes of aryl ring stretching. The treatment in the cosolvent led to significant changes in the C═O bonds, in the 1750−1610 cm^{-1} range. Overall, the Raman and nanoIR data are indicative of a rearrangement of lignin to expose aryl-ethers for cleavage during reaction in THF−water cosolvent, which is in line with the MD simulations.

Upon addition of 0.05 M dilute sulfuric acid to the cosolvent reactions at 160 °C (equivalent to how CELF pretreatment is performed), the hardwood slices contained only bands consistent with cellulose, as shown in Figure S7. This band has previously been assigned to the H−O−H angle vibration of water in cellulose.[98] To corroborate the observed disappearance of lignin at the nanoscale after dilute acid cosolvent reaction, we supplemented the nanoIR data by collecting compositional data from cosolvent and aqueous-only treated hardwood *Acer* solids after reaction in a 1 L vessel (Table S2). As shown in Table S2, cosolvent reaction in the absence of acid produced a solid material that still retained a majority of the carbohydrates, and a small amount of lignin was removed. However, with addition of as little as 0.5 wt % or 0.05 M dilute sulfuric acid into the cosolvent mixture, as much as 83% of the lignin and 95% of the hemicellulose were removed from the solids after only 25 min of reaction, suggesting that the mechanism for lignin extraction required both molecular rearrangement and dilute acid fragmentation. In the aqueous-only reactions, lignin was present in abundance after both nonacid and dilute-acid reactions with a majority of the mass loss due to the hydrolysis of the hemicellulose sugars.

Cosolvent Removal of Hemicellulose and Lignin Allows for Higher Sustained Enzymatic Hydrolysis Rates. Hemicellulose and lignin are known to contribute to the overall recalcitrance of biomass to microbial or enzymatic breakdown, severely affecting the accessibility, functionality, and activity of cellulolytic enzymes on cellulose in biomass.[99,100] Chemical pretreatment by removing one or both of these fractions can potentially lower production costs of second generation biofuels by reducing the amount of enzymes that are needed to achieve high sugar yields.[101] To investigate what impact hemicellulose and lignin removal from biomass have on the rate of enzymatic hydrolysis, we prepared several control samples from *Acer* wood chips, otherwise known as maple wood, and compared them to THF−water CELF pretreated *Acer*. As shown in Figure S8(iv), *Acer* and *Populus* varieties of hardwoods do not differ in their enzymatic

DOI: 10.1021/jacs.8b10242
J. Am. Chem. Soc. 2019, 141, 12545−12557

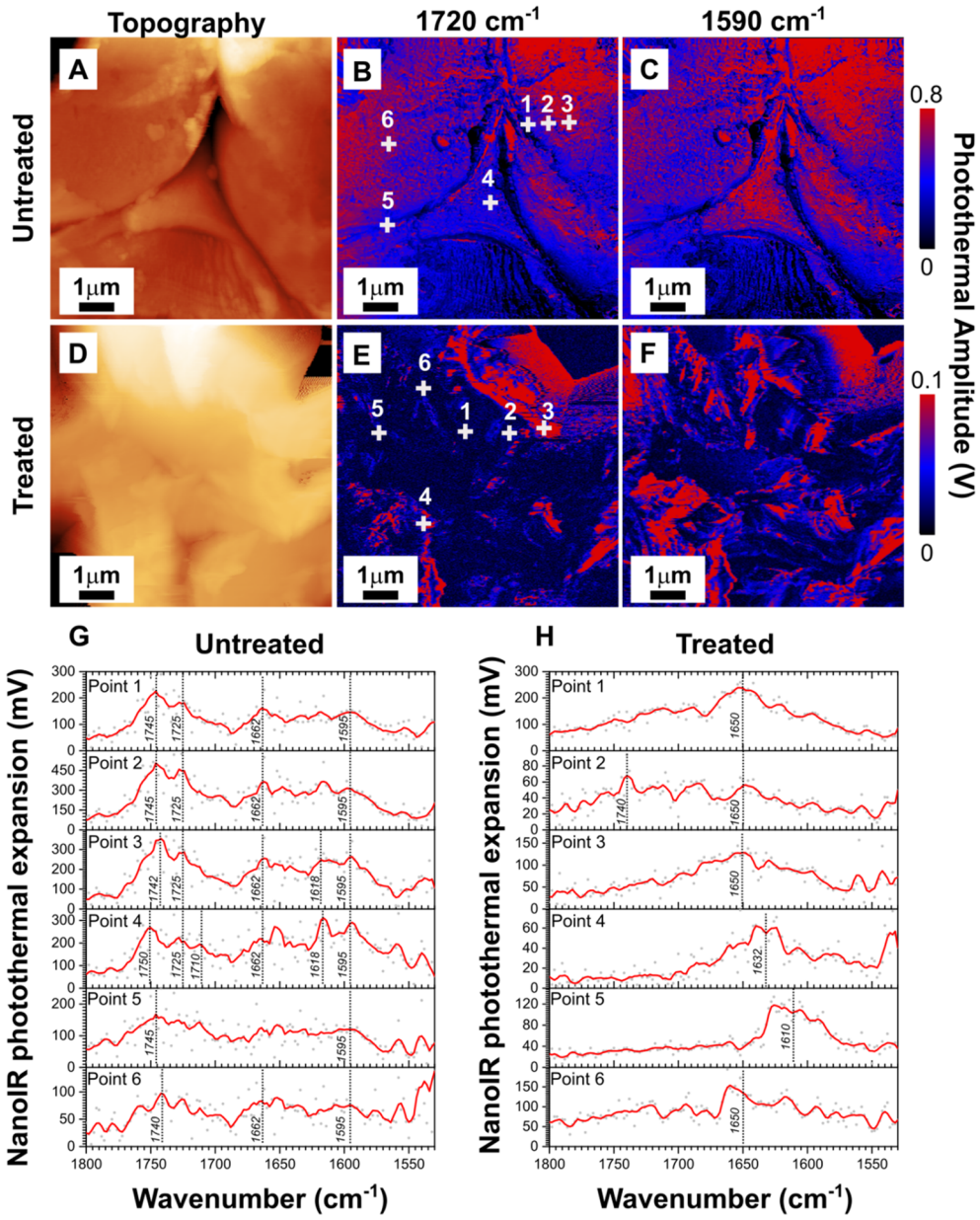

Figure 3. (A,D) Topography images of a cell corner in an untreated hardwood *Populus* cross section (A) and the cosolvent reacted cross section (D). (B,C) NanoIR maps of the same cell corner in an untreated *Populus* cross section at 1720 and 1590 cm^{-1}. (E,F) NanoIR maps of the cell corner in a cosolvent reacted *Populus* cross section at 1720 and 1590 cm^{-1}. (G) Local IR spectra obtained at selected regions across the cell wall including the secondary wall (points 1−3, 6), middle lamella (point 5), and cell corner (point 4). (H) Local IR spectra obtained at selected regions across the cell wall seemingly corresponding to the position of the secondary wall (points 1−3, 6), middle lamella (point 5), and cell corner (point 4).

digestibility, so both can be interchangeable in practice. For the production of the control samples, aqueous-only dilute sulfuric acid (DSA) pretreatment and sodium chlorite delignification were performed. After DSA pretreatment, 97% of the hemicellulose from *Acer* was removed, producing the hemicellulose-free (H-) *Acer* control sample. After sodium chlorite delignification, 98% of the lignin from *Acer* was removed producing the lignin-free (L-) *Acer* control sample. We further delignified H- *Acer* using the same sodium chlorite procedure to produce hemicellulose and lignin-free (H-L-) *Acer*. Rather than using highly processed Avicel cellulose, we produced H-L-*Acer* as a more relevant cellulose control to find out how the separate but deliberate removal methods for lignin and hemicellulose compare to CELF pretreated *Acer*. The enzymatic hydrolysis runs were performed using Accellerase enzyme cocktail, first at 5 mg-protein/g-glucose enzyme loadings, to find out the total % glucose yields after 5 days of incubation shown in Table 1. L-, H-L-, as well as CELF pretreated substrates achieved the highest glucose yields, indicating that lignin content was the primary factor to improving total enzymatic digestibility of the substrate, whereas removal of hemicellulose was a secondary factor with less of an impact toward higher glucose yield than lignin removal (Table 1 and Figure S8). Interestingly, with near complete removal of hemicellulose and lignin, as represented by H-L- *Acer*, this control substrate did not actually outperform CELF. Similar to the findings of another study, the near complete (>95%) removal of lignin from biomass could

DOI: 10.1021/jacs.8b10242
J. Am. Chem. Soc. 2019, 141, 12545−12557

Table 1. Compositions of Unpretreated, H-, L-, H-L-, and CELF Pretreated *Acer* Wood Chips and Final Glucose Yields Obtained after 5 days of Enzymatic Hydrolysis, Comparing Composition to Enzymatic Digestibility

substrate	glucan, %	xylan, %	K-lignin, %	glucose yield,[a] %
unpretreated *Acer*	45.7	20.3	24.4	2.9
hemicellulose-free (H-) *Acer*	63.3	2.1	32.6	20.4
lignin-free (L-) *Acer*	55.2	22.1	1.7	32.0
hemicellulose-free and lignin-free (H-L-) *Acer*	96.4	3.1	0	79.5
CELF pretreated *Acer*	89.1	2.3	8.1	98.6

[a]After 5 days of incubation with Accellerase 1500 at an enzyme loading of 5 mg-protein g-glucan-in-raw^{-1}.

actually result in a total collapse of the biomass macrostructure, leading to reduced enzyme accessibility within the cellulose fibers and slower hydrolysis.[102] Although CELF was capable of removing a majority of the lignin, it did not remove some of the lignin that may have been essential structural lignin (8−12 wt % of pretreated material), thus achieving significantly higher glucose yields than H-L- *Acer* after 5 days of incubation (Table 1).

Next, we compared the rate of enzymatic hydrolysis (Figure 4) for each of the four samples over the entire course of the

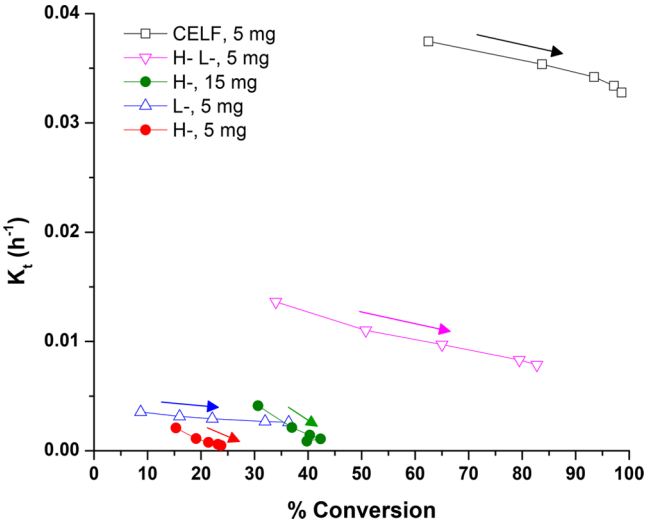

Figure 4. Change in fractal kinetic rate parameter, k_t, with respect to percent total glucan conversion during enzymatic hydrolysis comparing CELF pretreated solids to lignin-free or hemicellulose-free control samples. For hemicellulose-free *Acer* (H-) sample, incubation at enzyme loadings of both 5 and 15 mg protein/g glucan is shown. For lignin-free (L-), hemicellulose and lignin-free (H-L-), and CELF *Acer*, incubation at an enzyme loading of 5 mg protein/g glucan is shown. Color matched trailing arrows above the lines indicate the decay of the fractal rate parameter as glucan conversion proceeds.

incubation period to elucidate two important factors: (1) initial substrate accessibility and (2) the change of hydrolysis rate over glucan conversion. For this we fitted the glucan conversion of each material substrate to a fractal kinetic model, as described in the methods section and shown in Figure S8. The fractal model uniquely employs a transient rate parameter, k^t, that is dependent on a fractal time exponent, t^h, which can infer enzyme−cellulose binding efficiency and reveal how substrate differences can impact the rate of enzymatic hydrolysis.[72] The higher value of k^t corresponds to a higher total enzymatic hydrolysis rate. As hydrolysis continues and more glucan from the substrate is converted to glucose, enzyme performance typically suffers and can be observed in a fractal model by a decay in k^t as less glucan is available to the substrate-bound enzymes and potential enzyme deactivation. As shown in Figure 4, the H-L- *Acer* and CELF *Acer* had both the highest initial and sustained rates k_t over total % glucan conversion. Furthermore, for the biomass substrates containing little or no lignin (CELF, H-L-, and L- *Acer*), k_t decayed at a much slower rate over % total conversion than substrates with only hemicellulose removed. The distinctly flatter slope observed from the CELF, L-, and H-L- substrates, as indicated by the trailing arrows above each line in Figure 4 as glucan conversion increased, indicated that the removal of lignin was key to sustaining the rate of enzyme activity on the substrates over long incubation times or increasing glucan conversion. We further evaluated enzyme binding effects toward each of the prepared substrates by measuring the concentration of total protein in the liquid phase before and after performing enzymatic hydrolysis of each of the substrates (data shown in Table S4). Following complete hydrolysis of cellulose in H- *Acer*, the final free protein concentration in the liquid phase was reduced by 39% from the start of enzymatic hydrolysis, suggesting that a significant amount of enzyme had been nonproductively bound to the substrate residuals and lost. For CELF pretreated *Acer*, we found less than 3% change in free protein concentration in the liquid phase befcore or after enzymatic hydrolysis of the samples. The complete conservation of total free protein concentration in the liquid before and after incubation of cosolvent treated CELF *Acer* indicated that the substrate does not trap the enzyme and total enzyme activity is preserved. As observed in Figure 4, the low lignin and cellulose-rich nature of cosolvent treated CELF *Acer* supports the behavior of the hydrolysis rates: Higher conservation of free protein after hydrolysis indicated little to no loss of enzyme activity, typically suffered by unproductive binding to lignin, and the much slower decay of the transient rate parameter explains the sustained hydrolysis rates over the entire conversion of cellulose to glucose. The results also reveal that materials containing high lignin content are more susceptible to nonproductively binding enzymes that reduce enzyme activity and lead to the decay of hydrolysis rate over conversion. Total conservation of enzyme mass after hydrolysis further enables enzyme recycling or reuse. Furthermore, differences in the cellulose crystallinity and degree of polymerization for H- *Acer* and CELF *Acer* samples were determined to be minimal (comparison shown in Table S5).

Cosolvent Pretreatment with Dilute Acid Promotes Significant Lignin Depolymerization. The question then arises as to whether the physical modifications in the extracted lignin structure and bulk level delignification described above are accompanied by chemical modifications as a result of the interactions with the cosolvent environment. To evaluate this possibility, we used GPC and NMR techniques to analyze the structure of lignin solubilized and extracted from *Acer* by THF−water cosolvent reaction with dilute sulfuric acid, as practiced during CELF pretreatment. A highly pure lignin, solubilized during CELF pretreatment, can be recovered by precipitation upon removal and recovery of THF from the postpretreatment liquor by boiling. We then compared this

DOI: 10.1021/jacs.8b10242
J. Am. Chem. Soc. 2019, 141, 12545−12557

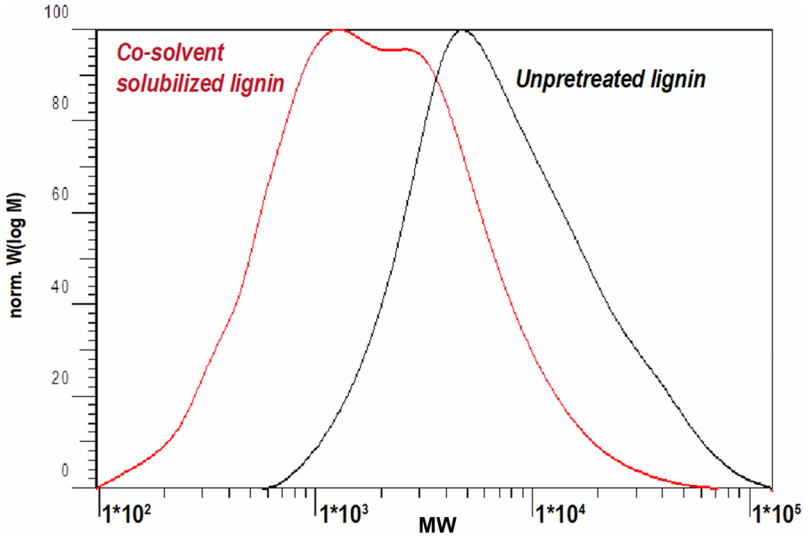

Figure 5. Molecular weight distribution of lignin from unpretreated *Acer* (control) and acidic cosolvent solubilized lignin from CELF. Lignin molecular weight decreases by ∼80% after CELF.

CELF lignin with native *Acer* lignin and lignin bound to biomass pretreated using aqueous-only dilute sulfuric acid pretreated at the same conditions as CELF (comparison shown in Table S3). The GPC analysis reveals that the molecular weight of solubilized lignin was reduced by ∼80% as compared to that from the unpretreated *Acer* control (Figure 5), indicating that solubilized lignin was highly fragmented after the acidic cosolvent reaction. Moreover, HSQC, ^{13}C, and ^{31}P NMR were applied to determine the chemical structures of lignin (Figure S9) showing a decrease of about ∼70% of total *β-O*-4 linkage content in the solubilized lignin as compared to the untreated polymer. A peak at around 152 ppm in the ^{13}C NMR spectrum (Figure S9B), attributed to the C3/5 in the etherified syringyl unit, was significantly reduced for the solubilized lignin, suggesting that etherified syringyl units (i.e., syringyl *β-O*-4 linkage) were very reactive and largely cleaved upon acidic cosolvent reaction. As compared to the lignin from the raw material, the ratio of the aromatic C−C bonds to aromatic C−H bonds for the lignin from CELF and dilute acid aqueous reaction both increased, indicating the occurrence of C−C condensed bond formation under both pretreatment conditions (Figure S9B). However, the ratio of the aromatic C−C bonds to aromatic C−H bonds for the CELF lignin was much less than the lignin from aqueous-only dilute acid pretreatment, suggesting that THF helped to reduce the aromatic C−C bond formation related to condensation products. Furthermore, the cleavage of the *β*-O-4 aryl ether bonds was supported by ^{31}P NMR data (Figure S9C), which resulted in a dramatic increase in phenolic OH groups, both from guaiacyl (∼60% increase) and from syringyl units (>10-fold increase), in the liquid fraction. These changes are in line with the changes in C═O and C═C bonds observed with nanoIR.

Under acidic conditions of CELF pretreatment, the predominant reactions in lignin are competitive fragmentation by acidolysis of aryl-ether (primarily *β*-O-4) linkages and repolymerization by acid-catalyzed condensation.[103,104] While the former reaction results in the formation of new phenolic end groups and decreased molecular weights of lignin, the latter gives rise to a new carbon−carbon linkage between two lignin units resulting in an undesirable increase in molecular size negatively impacting its functionality. The apparent shift of peak in the lignin molecular weight distribution to low molecular weights (as shown in Figure 5) demonstrated a significant decrease in molecular size, suggesting fragmentation was the dominant reaction in CELF process. The results suggested that the cosolvent reaction significantly favored acid-catalyzed depolymerization of native lignin while limiting its condensation, leading to low molecular weight products. ^{13}C NMR analysis showed that the ratio of the aromatic C−C bonds to aromatic C−H bonds for the CELF lignin is significantly less than the lignin from dilute acid pretreatment without THF, indicating less formation of C−C condensed bonds under CELF pretreatment condition. Evidence was consistent with the MD simulations, which showed that lignin molecules become individually solvated in the cosolvent environment, whereas they aggregate in water (Figures 1 and S1).

■ DISCUSSION

The results presented here describe a set of molecular principles driving the efficient breakdown of biomass resulting from its molecular interactions with cosolvents THF−water. THF−water is highlighted here as a multifunctional cosolvent pair supporting the lignin-first approach toward achieving total breakdown and utilization of biomass. THF complements aqueous dilute acid pretreatment of biomass to enable clean fractionation of depolymerized lignin while it is displaced from the plant cell wall. After cosolvent treatment, the remaining cellulose-rich material can be completely digested by hydrolytic enzymes unencumbered by nonstructural lignin inhibitors. Because the lignin solubilized by THF is fully dissolved in the liquid phase, it can be recovered at high purity as a technical grade precursor serving a wide range of lignin valorization techniques. Recent advances have been made in understanding acid-catalyzed lignin depolymerization[105] with the aim of achieving lignin breakdown together with gaining access to carbohydrates in lignocellulose. However, for typical acidic pretreatment conditions in water, achieving high degrees of lignin depolymerization is challenging due to concurrent lignin recondensation reactions and lignin redeposition onto cellulose.[106] While previous studies have suggested that the

DOI: 10.1021/jacs.8b10242
J. Am. Chem. Soc. 2019, 141, 12545−12557

addition of a protecting agent can help to stabilize lignin for subsequent catalytic depolymerization, these methods still require separate strategies for the depolymerization of lignin, recovery of sugars, and handling of sugar breakdown products.[107] As such, the amalgamation of effective lignin depolymerization combined with obtaining high sugar yields for biofuel production at the commercial scale has yet to be demonstrated. This multiscale study illustrates the importance of looking at lignin conformation and its interaction with cellulose in cosolvent environments as key mechanisms for achieving high yield recovery of both lignin and sugars as valuable chemical precursors. The THF−water cosolvent pair is a highly effective "theta" solvent for lignin that can coordinate with and expose native interlignin bonds to facilitate their cleavage during dilute acid pretreatment (Figure S1 and movie S1), resulting in the liberation and unfettered access to both lignin and cellulose in a single system. These results support previous studies that have shown how CELF pretreated biomass can separate lignin and achieve high total sugar utilization toward industrially relevant bioethanol titers while reducing enzyme demand by up to 90%,[45,46] thus demonstrating that cosolvent-based technology is an ideal candidate for the study of molecular principles that synergistically promote effective biomass deconstruction. Together, nanoscale functional imaging, NMR, and MD simulations reveal that lignin molecular rearrangement is near cellulose in a cosolvent environment, with aryl ring residues exposed in the plant cell walls, whereas the addition of dilute acid to the reaction results in lignin removal from the plant cell wall and the solubilization of hemicellulose. Further, the decrease in the number of aryl-ether interlignin linkages in the recovered lignin indicates that lignin undergoes significant depolymerization by acid-catalyzed hydrolysis, likely facilitated by lignin adopting extended macromolecular configurations in which linkages are significantly exposed to the solvent. Observations made at various time points with Raman and localized inspection of the cell wall layers with nanoIR measurements suggest that the nature and quantity of lignin removed could possibly be tuned by selecting different treatments or reaction times. After acid-catalyzed depolymerization has taken place, lignin fragments are individually solvated in the cosolvent, thus leading to reduced formation of aromatic C−C linkages result from certain condensation reactions. Figures 5 and S9C show evidence of lignin depolymerization from reduced molecular weight and increased phenolic group content in syringyl and guaiacyl units, indicating extensive cleavage of aryl ether interunit linkages. Further, GPC data indicate that lignin fragmentation is dominant, and nanoIR data in Figure 3 further demonstrate how extracted lignin does not simply redeposit onto the cell wall surface. Finally, with the majority of lignin extracted from the bulk of the biomass, facile enzymatic digestion of cellulose is achievable, without any significant loss of enzyme activity (Figures 4 and S8) or unproductive binding, suggesting that any enzymes added to digest CELF-pretreated material may be effectively recycled without compromising subsequent hydrolysis performance. Thus, advanced pretreatment methods employing multifunctional cosolvents will allow simultaneous processing of sugar and lignin fractions from biomass to more economically prepare valuable chemical precursors suitable for further valorization to biofuels and biochemicals, without the need to employ expensive and complicated multistage processes.

CONCLUSIONS

The identification and use of multifunctional cosolvents to aid in the pretreatment and fractionation of biomass ushers in a new age of integrative process design to incorporate both lignin and cellulose deconstruction to improve total biomass utilization. The multiscale approach applied here reveals the importance of lignin manipulation by cosolvents toward driving the combinatory factors enabling the complete hydrolysis of cellulose. The coupling of physical (changes in lignin conformations and solvent organization, as shown previously[53−57]) and chemical (catalysis of bond cleavage) processes emerges as a key principle behind optimal pretreatment design. These results portend a paradigm shift in the field of biomass conversion away from solely addressing cellulose recalcitrance, hemicellulose inhibition, or lignin extraction/refining and toward employing a rationally selected solvent marriage capable of synergistically deconstructing whole biomass systems, so as to yield unfettered access to both sugars and lignin for amenable valorization.

ASSOCIATED CONTENT

Supporting Information

The Supporting Information is available free of charge on the ACS Publications website at DOI: 10.1021/jacs.8b10242.

Figures S1−S9 and Tables S1−S5 (PDF)
Movie S1 (MOV)

AUTHOR INFORMATION

Corresponding Author

*E-mail: ccai@engr.ucr.edu.

ORCID

Barmak Mostofian: 0000-0003-0568-9866
Micholas Dean Smith: 0000-0002-0777-7539
Xiaolin Cheng: 0000-0002-7396-3225
Arthur J. Ragauskas: 0000-0002-3536-554X
Jeremy C. Smith: 0000-0002-2978-3227
Loukas Petridis: 0000-0001-8569-060X
Charles M. Cai: 0000-0002-5047-0815

Notes

The authors declare no competing financial interest.

ACKNOWLEDGMENTS

We acknowledge support from the Office of Biological and Environmental Research in the Department of Energy (DOE) Office of Science through the BioEnergy Science Center (BESC) and the Center for Bioenergy Innovation (CBI) at Oak Ridge National Laboratory. The award of a fellowship to the lead author by the National Center for Sustainable Transportation made his participation in this project possible. We also acknowledge the support from the Genomic Science Program, Office of Biological and Environmental Research, U.S. Department of Energy (contract FWP ERKP752), and funding from the Southeastern Regional Sun Grant Center at the University of Tennessee through a grant provided by the U.S. Department of Agriculture (award number 2014-38502-22598). This research used resources of the Oak Ridge Leadership Computing Facility under an INCITE award (contract FWP DE-AC05-00OR22725) and the Compute and Data Environment for Science (CADES) resources at the Oak Ridge National Laboratory. We also acknowledge the Center for Environmental Research and Technology (CE-

DOI: 10.1021/jacs.8b10242
J. Am. Chem. Soc. 2019, 141, 12545−12557

CERT) of the Bourns College of Engineering at University of California Riverside for providing the facilities and the Ford Motor Co. for funding the Chair in Environmental Engineering that facilitates projects such as this one.

REFERENCES

(1) van Renssen, S. An energy revolution. *Nat. Clim. Change* **2012**, *2* (1), 19−20.
(2) Trancik, J. Renewable Energy: Back the Renewables Boom. *Nature* **2014**, *507*, 300−302.
(3) Elliott, D. A Balancing Act for Renewables. *Nature Energy* **2016**, *1*, 15003.
(4) Jeffries, E. News feature: Freeing fossil fuels. *Nat. Clim. Change* **2016**, *6* (2), 125−126.
(5) Lynd, L. R.; Cushman, J. H.; Nichols, R. J.; Wyman, C. E. Fuel ethanol from cellulosic biomass. *Science (Washington, DC, U. S.)* **1991**, *251* (4999), 1318−1323.
(6) Rostrup-Nielsen, J. Making Fuels from Biomass. *Science* **2005**, *308* (5727), 1421−1422.
(7) Dodds, D.; Gross, R. Chemicals from Biomass. *Science* **2007**, *318* (5854), 1250−1251.
(8) Ragauskas, A.; Williams, C.; Davison, B.; Britovsek, G.; Cairney, J.; Eckert, C.; Frederick, W.; Hallett, J.; Leak, D.; Liotta, C.; Mielenz, J.; Murphy, R.; Templer, R.; Tschaplinski, T. The path forward for biofuels and biomaterials. *Science (Washington, DC, U. S.)* **2006**, *311* (5760), 484−489.
(9) Simmons, B.; Loque, D.; Blanch, H. Next-generation biomass feedstocks for biofuel production. *Genome biology* **2008**, *9* (12), 242.
(10) Himmel, M. E.; Ding, S. Y.; Johnson, D. K.; Adney, W. S.; Nimlos, M. R.; Brady, J. W.; Foust, T. D. Biomass recalcitrance: engineering plants and enzymes for biofuels production. *Science* **2007**, *315* (5813), 804−7.
(11) Converse, A. O.; Matsuno, R.; Tanaka, M.; Taniguchi, M. A Model of Enzyme Adsorption and Hydrolysis of Microcrystalline Cellulose with Slow Deactivation of the Adsorbed Enzyme. *Biotechnol. Bioeng.* **1988**, *32* (1), 38−45.
(12) Holtzapple, M.; Cognata, M.; Shu, Y.; Hendrickson, C. Inhibition of Trichoderma-Reesei Cellulase by Sugars and Solvents. *Biotechnol. Bioeng.* **1990**, *36* (3), 275−287.
(13) Eriksson, T.; Karlsson, J.; Tjerneld, F. A model explaining declining rate in hydrolysis of lignocellulose substrates with cellobiohydrolase I (Cel7A) and endoglucanase I (Cel7B) of Trichoderma reesei. *Appl. Biochem. Biotechnol.* **2002**, *101* (1), 41−60.
(14) Scheiding, W.; Thoma, M.; Ross, A.; Schugerl, K. Modeling of the Enzymatic-Hydrolysis of Cellobiose and Cellulose by a Complex Enzyme Mixture of Trichoderma-Reesei Qm 9414. *Appl. Microbiol Biot* **1984**, *20* (3), 176−182.
(15) Vermaas, J. V.; Petridis, L.; Qi, X. H.; Schulz, R.; Lindner, B.; Smith, J. C. Mechanism of lignin inhibition of enzymatic biomass deconstruction. *Biotechnol Biofuels* **2015**, *8*, 1 DOI: 10.1186/s13068-015-0379-8.
(16) Zhao, X.; Zhang, L.; Liu, D. Biomass recalcitrance. Part II: Fundamentals of different pre-treatments to increase the enzymatic digestibility of lignocellulose. *Biofuels, Bioprod. Biorefin.* **2012**, *6* (5), 561−579.
(17) Kumar, R.; Wyman, C. E. Strong cellulase inhibition by Mannan polysaccharides in cellulose conversion to sugars. *Biotechnol. Bioeng.* **2014**, *111* (7), 1341−53.
(18) Kumar, R.; Wyman, C. E. Effect of xylanase supplementation of cellulase on digestion of corn stover solids prepared by leading pretreatment technologies. *Bioresour. Technol.* **2009**, *100* (18), 4203−13.
(19) Lloyd, T. A.; Wyman, C. E. Combined sugar yields for dilute sulfuric acid pretreatment of corn stover followed by enzymatic hydrolysis of the remaining solids. *Bioresour. Technol.* **2005**, *96* (18), 1967−1977.
(20) Kumar, R.; Mago, G.; Balan, V.; Wyman, C. E. Physical and chemical characterizations of corn stover and poplar solids resulting from leading pretreatment technologies. *Bioresour. Technol.* **2009**, *100* (17), 3948−62.
(21) Pu, Y.; Hu, F.; Huang, F.; Davison, B. H.; Ragauskas, A. J. Assessing the molecular structure basis for biomass recalcitrance during dilute acid and hydrothermal pretreatments. *Biotechnol. Biofuels* **2013**, *6* (1), 15.
(22) Linger, J. G.; Vardon, D. R.; Guarnieri, M. T.; Karp, E. M.; Hunsinger, G. B.; Franden, M. A.; Johnson, C. W.; Chupka, G.; Strathmann, T. J.; Pienkos, P. T.; Beckham, G. T. Lignin valorization through integrated biological funneling and chemical catalysis. *Proc. Natl. Acad. Sci. U. S. A.* **2014**, *111* (33), 12013−12018.
(23) Ragauskas, A. J.; Beckham, G. T.; Biddy, M. J.; Chandra, R.; Chen, F.; Davis, M. F.; Davison, B. H.; Dixon, R. A.; Gilna, P.; Keller, M.; Langan, P.; Naskar, A. K.; Saddler, J. N.; Tschaplinski, T. J.; Tuskan, G. A.; Wyman, C. E. Lignin Valorization: Improving Lignin Processing in the Biorefinery. *Science* **2014**, *344* (6185), 709.
(24) Chum, H. L.; Parker, S. K.; Feinberg, D. A.; Wright, J. D.; Rice, P. A.; Sinclair, S. A.; Glasser, W. G. Economic contribution of lignins to ethanol production from biomass; SERI/TR-231-2488; Other: ON: DE850088145 United States Other: ON: DE850088145 NTIS, PC A06/MF A01. NREL English; Solar Energy Research Inst., Golden, CO, 1985; p Medium: X; Size: Pages: 102.
(25) Nguyen, N. A.; Barnes, S. H.; Bowland, C. C.; Meek, K. M.; Littrell, K. C.; Keum, J. K.; Naskar, A. K. A path for lignin valorization via additive manufacturing of high-performance sustainable composites with enhanced 3D printability. *Science Advances* **2018**, *4* (12), No. eaat4967.
(26) Zhao, X.; Cheng, K.; Liu, D. Organosolv pretreatment of lignocellulosic biomass for enzymatic hydrolysis. *Appl. Microbiol. Biotechnol.* **2009**, *82* (5), 815−27.
(27) Galkin, M. V.; Samec, J. S. M. Lignin Valorization through Catalytic Lignocellulose Fractionation: A Fundamental Platform for the Future Biorefinery. *ChemSusChem* **2016**, *9* (13), 1544−1558.
(28) Rodriguez, A.; Salvachúa, D.; Katahira, R.; Black, B. A.; Cleveland, N. S.; Reed, M. L.; Smith, H.; Baidoo, E. E.; Keasling, J. D.; Simmons, B. A. Base-catalyzed depolymerization of solid lignin-rich streams enables microbial conversion. *ACS Sustainable Chem. Eng.* **2017**, *5*, 8171.
(29) Alizadeh, H.; Teymouri, F.; Gilbert, T. I.; Dale, B. E. Pretreatment of switchgrass by ammonia fiber explosion (AFEX). *Appl. Biochem. Biotechnol.* **2005**, *121*, 1133−1141.
(30) Balan, V.; Bals, B.; Chundawat, S. P. S.; Marshall, D.; Dale, B. E. Lignocellulosic Biomass Pretreatment Using AFEX. *Methods Mol. Biol.* **2009**, *581*, 61−77.
(31) Huijgen, W. J. J.; Smit, A. T.; de Wild, P. J.; den Uil, H. Fractionation of wheat straw by prehydrolysis, organosolv delignification and enzymatic hydrolysis for production of sugars and lignin. *Bioresour. Technol.* **2012**, *114*, 389−398.
(32) Johansson, A.; Aaltonen, O.; Ylinen, P. Organosolv Pulping - Methods and Pulp Properties. *Biomass* **1987**, *13* (1), 45−65.
(33) Lora, J. H.; Aziz, S. Organosolv Pulping - a Versatile Approach to Wood Refining. *Tappi J.* **1985**, *68*, 94−97.
(34) Pan, X. J.; Arato, C.; Gilkes, N.; Gregg, D.; Mabee, W.; Pye, K.; Xiao, Z. Z.; Zhang, X.; Saddler, J. Biorefining of softwoods using ethanol organosolv pulping: Preliminary evaluation of process streams for manufacture of fuel-grade ethanol and co-products. *Biotechnol. Bioeng.* **2005**, *90* (4), 473−481.
(35) Pan, X. J.; Gilkes, N.; Kadla, J.; Pye, K.; Saka, S.; Gregg, D.; Ehara, K.; Xie, D.; Lam, D.; Saddler, J. Bioconversion of hybrid poplar to ethanol and co-products using an organosolv fractionation process: Optimization of process yields. *Biotechnol. Bioeng.* **2006**, *94* (5), 851−861.
(36) Zhang, Z. Y.; Harrison, M. D.; Rackemann, D. W.; Doherty, W. O. S.; O'Hara, I. M. Organosolv pretreatment of plant biomass for enhanced enzymatic saccharification. *Green Chem.* **2016**, *18* (2), 360−381.
(37) Bals, B.; Wedding, C.; Balan, V.; Sendich, E.; Dale, B. Evaluating the impact of ammonia fiber expansion (AFEX) pretreat-

DOI: 10.1021/jacs.8b10242
J. Am. Chem. Soc. 2019, 141, 12545−12557

ment conditions on the cost of ethanol production. *Bioresour. Technol.* **2011**, *102* (2), 1277−1283.
(38) Kristensen, J. B.; Felby, C.; Jorgensen, H. Yield-determining factors in high-solids enzymatic hydrolysis of lignocellulose. *Biotechnol Biofuels* **2009**, *2*, 11.
(39) Shuai, L.; Yang, Q.; Zhu, J. Y.; Lu, F. C.; Weimer, P. J.; Ralph, J.; Pan, X. J. Comparative study of SPORL and dilute-acid pretreatments of spruce for cellulosic ethanol production. *Bioresour. Technol.* **2010**, *101* (9), 3106−3114.
(40) Wang, G. S.; Pan, X. J.; Zhu, J. Y.; Gleisner, R.; Rockwood, D. Sulfite Pretreatment to Overcome Recalcitrance of Lignocellulose (SPORL) for Robust Enzymatic Saccharification of Hardwoods. *Biotechnol. Prog.* **2009**, *25* (4), 1086−1093.
(41) Zhu, J. Y.; Pan, X. J.; Wang, G. S.; Gleisner, R. Sulfite pretreatment (SPORL) for robust enzymatic saccharification of spruce and red pine. *Bioresour. Technol.* **2009**, *100* (8), 2411−2418.
(42) Xu, F.; Sun, J.; Konda, N. V. S. N. M.; Shi, J.; Dutta, T.; Scown, C. D.; Simmons, B. A.; Singh, S. Transforming biomass conversion with ionic liquids: process intensification and the development of a high-gravity, one-pot process for the production of cellulosic ethanol. *Energy Environ. Sci.* **2016**, *9* (3), 1042−1049.
(43) Ragauskas, A. J.; Williams, C. K.; Davison, B. H.; Britovsek, G.; Cairney, J.; Eckert, C. A.; Frederick, W. J.; Hallett, J. P.; Leak, D. J.; Liotta, C. L.; Mielenz, J. R.; Murphy, R.; Templer, R.; Tschaplinski, T. The path forward for biofuels and biomaterials. *Science* **2006**, *311* (5760), 484−489.
(44) Alonso, D. M.; Wettstein, S. G.; Dumesic, J. A. Gamma-valerolactone, a sustainable platform molecule derived from lignocellulosic biomass. *Green Chem.* **2013**, *15* (3), 584−595.
(45) Nguyen, T. Y.; Cai, C. M.; Kumar, R.; Wyman, C. E. Co-solvent Pretreatment Reduces Costly Enzyme Requirements for High Sugar and Ethanol Yields from Lignocellulosic Biomass. *ChemSusChem* **2015**, *8*, 1716.
(46) Nguyen, T. Y.; Cai, C. M.; Kumar, R.; Wyman, C. E. Overcoming factors limiting high-solids fermentation of lignocellulosic biomass to ethanol. *Proc. Natl. Acad. Sci. U. S. A.* **2017**, *114* (44), 11673−11678.
(47) Cai, C. M.-Z. Co-Solvent Enhanced Production of Platform Fuel Precursors From Lignocellulosic Biomass. PhD Thesis. University of California Riverside, 2014.
(48) Cai, C. M.; Nagane, N.; Kumar, R.; Wyman, C. E. Coupling metal halides with a co-solvent to produce furfural and 5-HMF at high yields directly from lignocellulosic biomass as an integrated biofuels strategy. *Green Chem.* **2014**, *16* (8), 3819−3829.
(49) Cai, C. M.; Zhang, T. Y.; Kumar, R.; Wyman, C. E. THF co-solvent enhances hydrocarbon fuel precursor yields from lignocellulosic biomass. *Green Chem.* **2013**, *15* (11), 3140−3145.
(50) Seemala, B.; Meng, X.; Parikh, A.; Nagane, N.; Kumar, R.; Wyman, C. E.; Ragauskas, A.; Christopher, P.; Cai, C. M. Hybrid Catalytic Biorefining of Hardwood Biomass to Methylated Furans and Depolymerized Technical Lignin. *ACS Sustainable Chem. Eng.* **2018**, *6* (8), 10587−10594.
(51) Thomas, V. A.; Donohoe, B. S.; Li, M.; Pu, Y.; Ragauskas, A. J.; Kumar, R.; Nguyen, T. Y.; Cai, C. M.; Wyman, C. E. Adding tetrahydrofuran to dilute acid pretreatment provides new insights into substrate changes that greatly enhance biomass deconstruction by Clostridium thermocellum and fungal enzymes. *Biotechnology for Biofuels* **2017**, *10*, 1 DOI: 10.1186/s13068-017-0937-3.
(52) Li, W.; Ghosh, A.; Bbosa, D.; Brown, R.; Wright, M. M. Comparative Techno-economic, Uncertainty and Life Cycle Analysis of Lignocellulosic Biomass Solvent Liquefaction and Sugar Fermentation to Ethanol. *ACS Sustainable Chem. Eng.* **2018**, *6* (12), 16515−16524.
(53) Mostofian, B.; Cai, C. M.; Smith, M. D.; Petridis, L.; Cheng, X. L.; Wyman, C. E.; Smith, J. C. Local Phase Separation of Co-solvents Enhances Pretreatment of Biomass for Bioenergy Applications. *J. Am. Chem. Soc.* **2016**, *138* (34), 10869−10878.
(54) Smith, M. D.; Cheng, X. L.; Petridis, L.; Mostofian, B.; Smith, J. C. Organosolv-Water Cosolvent Phase Separation on Cellulose and its Influence on the Physical Deconstruction of Cellulose: A Molecular Dynamics Analysis. *Sci. Rep-Uk* **2017**, *7*, 1 DOI: 10.1038/s41598-017-15048-7.
(55) Smith, M. D.; Mostofian, B.; Cheng, X.; Petridis, L.; Cai, C. M.; Wyman, C. E.; Smith, J. C. Cosolvent pretreatment in cellulosic biofuel production: effect of tetrahydrofuran-water on lignin structure and dynamics. *Green Chem.* **2016**, *18* (5), 1268−1277.
(56) Smith, M. D.; Petridis, L.; Cheng, X.; Mostofian, B.; Smith, J. C. Enhanced Sampling Simulation Analysis of the Structure of Lignin in the THF-Water Miscibility Gap. *Phys. Chem. Chem. Phys.* **2016**, *18*, 6394−6398.
(57) Smith, M. D.; Cai, C. M.; Cheng, X. L.; Petridis, L.; Smith, J. C. Temperature-dependent phase behaviour of tetrahydrofuran-water alters solubilization of xylan to improve co-production of furfurals from lignocellulosic biomass. *Green Chem.* **2018**, *20* (7), 1612−1620.
(58) Nishiyama, Y.; Langan, P.; Chanzy, H. Crystal Structure and Hydrogen-Bonding System in Cellulose Iβ from Synchrotron X-ray and Neutron Fiber Diffraction. *J. Am. Chem. Soc.* **2002**, *124* (31), 9074−9082.
(59) Petridis, L.; Schulz, R.; Smith, J. C. Simulation Analysis of the Temperature Dependence of Lignin Structure and Dynamics. *J. Am. Chem. Soc.* **2011**, *133* (50), 20277−20287.
(60) Gao, X.; Kumar, R.; Singh, S.; Simmons, B. A.; Balan, V.; Dale, B. E.; Wyman, C. E. Comparison of enzymatic reactivity of corn stover solids prepared by dilute acid, AFEX, and ionic liquid pretreatments. *Biotechnol. Biofuels* **2014**, *7* (1), 71.
(61) Guvench, O.; Hatcher, E.; Venable, R.; Pastor, R.; MacKerell, A. CHARMM Additive All-Atom Force Field for Glycosidic Linkages between Hexopyranoses. *J. Chem. Theory Comput.* **2009**, *5* (9), 2353−2370.
(62) Guvench, O.; Mallajosyula, S.; Raman, P.; Hatcher, E.; Vanommeslaeghe, K.; Foster, T.; Jamison, F.; MacKerell, A. CHARMM Additive All-Atom Force Field for Carbohydrate Derivatives and Its Utility in Polysaccharide and Carbohydrate−Protein Modeling. *J. Chem. Theory Comput.* **2011**, *7* (10), 3162−3180.
(63) Vorobyov, I.; Anisimov, V.; Greene, S.; Venable, R.; Moser, A.; Pastor, R.; MacKerell, A. Additive and Classical Drude Polarizable Force Fields for Linear and Cyclic Ethers. *J. Chem. Theory Comput.* **2007**, *3* (3), 1120−1133.
(64) Petridis, L.; Smith, J. C. A Molecular Mechanics Force Field for Lignin. *J. Comput. Chem.* **2009**, *30* (3), 457−467.
(65) Jorgensen, W.; Chandrasekhar, J.; Madura, J.; Impey, R.; Klein, M. Comparison of simple potential functions for simulating liquid water. *J. Chem. Phys.* **1983**, *79* (2), 926−935.
(66) Pronk, S.; Páll, S.; Schulz, R.; Larsson, P.; Bjelkmar, P.; Apostolov, R.; Shirts, M.; Smith, J.; Kasson, P.; van der Spoel, D.; Hess, B.; Lindahl, E. GROMACS 4.5: a high-throughput and highly parallel open source molecular simulation toolkit. *Bioinformatics* **2013**, *29* (7), 845−854.
(67) Humphrey, W.; Dalke, A.; Schulten, K. VMD: Visual molecular dynamics. *J. Mol. Graphics* **1996**, *14* (1), 33−38.
(68) Kumar, R.; Hu, F.; Hubbell, C. A.; Ragauskas, A. J.; Wyman, C. E. Comparison of laboratory delignification methods, their selectivity, and impacts on physiochemical characteristics of cellulosic biomass. *Bioresour. Technol.* **2013**, *130*, 372−381.
(69) Selig, M.; Weiss, N.; Ji, Y. Enzymatic Saccharification of Lignocellulosic Biomass: Laboratory Analytical Procedure (LAP): Issue Date, 3/21/2008; National Renewable Energy Laboratory: 2008.
(70) Nguyen, T. Y.; Cai, C. M.; Kumar, R.; Wyman, C. E. Co-solvent Pretreatment Reduces Costly Enzyme Requirements for High Sugar and Ethanol Yields from Lignocellulosic Biomass. *ChemSusChem* **2015**, *8* (10), 1716−1725.
(71) Mok, Y. K.; Arantes, V.; Saddler, J. N. A NaBH4 Coupled Ninhydrin-Based Assay for the Quantification of Protein/Enzymes During the Enzymatic Hydrolysis of Pretreated Lignocellulosic Biomass. *Appl. Biochem. Biotechnol.* **2015**, *176* (6), 1564−1580.

DOI: 10.1021/jacs.8b10242
J. Am. Chem. Soc. 2019, 141, 12545−12557

(72) Wang, Z.; Feng, H. Fractal kinetic analysis of the enzymatic saccharification of cellulose under different conditions. *Bioresour. Technol.* **2010**, *101* (20), 7995−8000.
(73) Dazzi, A.; Prater, C. B. AFM-IR: Technology and Applications in Nanoscale Infrared Spectroscopy and Chemical Imaging. *Chem. Rev.* **2017**, *117*, 5146.
(74) Sluiter, A.; Hames, B.; Ruiz, R.; Scarlata, C.; Sluiter, J.; Templeton, D.; Crocker, D. Determination of structural carbohydrates and lignin in biomass. *Laboratory Analytical Procedure* **2008**, *1617*, 1−16.
(75) Hallac, B. B.; Ragauskas, A. J. Analyzing cellulose degree of polymerization and its relevancy to cellulosic ethanol. *Biofuels, Bioprod. Biorefin.* **2011**, *5* (2), 215−225.
(76) Pu, Y. Q.; Chen, F.; Ziebell, A.; Davison, B. H.; Ragauskas, A. J. NMR Characterization of C3H and HCT Down-Regulated Alfalfa Lignin. *BioEnergy Res.* **2009**, *2* (4), 198−208.
(77) Ragauskas, A.; Pu, Y.; Samuel, R.; Jiang, N.; Fu, C.; Wang, Z.-Y. Structural Characterization of Lignin in Wild-Type versus COMT Down-Regulated Switchgrass. *Frontiers in Energy Research* **2014**, *1* (14), 1 DOI: 10.3389/fenrg.2013.00014.
(78) Pu, Y. Q.; Cao, S. L.; Ragauskas, A. J. Application of quantitative P-31 NMR in biomass lignin and biofuel precursors characterization. *Energy Environ. Sci.* **2011**, *4* (9), 3154−3166.
(79) Petridis, L.; Smith, J. C. Molecular-level driving forces in lignocellulosic biomass deconstruction for bioenergy. *Nature Reviews Chemistry* **2018**, *2* (11), 382−389.
(80) Lindner, B.; Petridis, L.; Schulz, R.; Smith, J. C. Solvent-Driven Preferential Association of Lignin with Regions of Crystalline Cellulose in Molecular Dynamics Simulation. *Biomacromolecules* **2013**, *14* (10), 3390−3398.
(81) Sun, Z.; Fridrich, B.; de Santi, A.; Elangovan, S.; Barta, K. Bright Side of Lignin Depolymerization: Toward New Platform Chemicals. *Chem. Rev.* **2018**, *118* (2), 614−678.
(82) Gray, S. R.; Peretti, S. W.; Lamb, H. H. Real-time monitoring of high-gravity corn mash fermentation using in situ raman spectroscopy. *Biotechnol. Bioeng.* **2013**, *110* (6), 1654−1662.
(83) Lupoi, J. S.; Gjersing, E.; Davis, M. F. Evaluating Lignocellulosic Biomass, Its Derivatives, and Downstream Products with Raman Spectroscopy. *Frontiers in Bioengineering and Biotechnology* **2015**, *3* (50), 1 DOI: 10.3389/fbioe.2015.00050.
(84) Agarwal, U. P. 1064 nm FT-Raman spectroscopy for investigations of plant cell walls and other biomass materials. *Frontiers in Plant Science* **2014**, *5* (490), 1 DOI: 10.3389/fpls.2014.00490.
(85) Gierlinger, N.; Schwanninger, M. Chemical Imaging of Poplar Wood Cell Walls by Confocal Raman Microscopy. *Plant Physiol.* **2006**, *140* (4), 1246−1254.
(86) Gierlinger, N.; Schwanninger, M. The potential of Raman microscopy and Raman imaging in plant research. *Spectroscopy* **2007**, *21* (2), 69−89.
(87) Gierlinger, N.; Keplinger, T.; Harrington, M. Imaging of plant cell walls by confocal Raman microscopy. *Nat. Protoc.* **2012**, *7*, 1694.
(88) Chundawat, S. P. S.; Donohoe, B. S.; da Costa Sousa, L.; Elder, T.; Agarwal, U. P.; Lu, F.; Ralph, J.; Himmel, M. E.; Balan, V.; Dale, B. E. Multi-scale visualization and characterization of lignocellulosic plant cell wall deconstruction during thermochemical pretreatment. *Energy Environ. Sci.* **2011**, *4* (3), 973−984.
(89) Agarwal, U. P.; McSweeny, J. D.; Ralph, S. A. FT−Raman Investigation of Milled-Wood Lignins: Softwood, Hardwood, and Chemically Modified Black Spruce Lignins. *J. Wood Chem. Technol.* **2011**, *31* (4), 324−344.
(90) ATALLA, R. H.; AGARWAL, U. P. Raman Microprobe Evidence for Lignin Orientation in the Cell Walls of Native Woody Tissue. *Science* **1985**, *227* (4687), 636−638.
(91) Agarwal, U. P. Raman imaging to investigate ultrastructure and composition of plant cell walls: distribution of lignin and cellulose in black spruce wood (Picea mariana). *Planta* **2006**, *224* (5), 1141.
(92) Agarwal, U. *Raman Spectroscopy of Lignin*; 1992; pp 162−176.
(93) Lähdetie, A.; Nousiainen, P.; Sipilä, J.; Tamminen, T.; Jääskeläinen, A.-S. Laser-induced fluorescence (LIF) of lignin and lignin model compounds in Raman spectroscopy. *Holzforschung*; 2013; Vol. *67*, p 531.
(94) Agarwal, U. P. An overview of Raman spectroscopy as applied to lignocellulosic materials. *Adv. Lignocellulosics Charact.* **1999**, 201−225.
(95) Marcott, C.; Lo, M.; Kjoller, K.; Prater, C.; Gerrard, D. P. Applications of AFM-IR—Diverse Chemical Composition Analyses at Nanoscale Spatial Resolution. *Microsc. Today* **2012**, *20* (6), 16−21.
(96) Gupta, B. S.; Jelle, B. P.; Gao, T. Wood facade materials ageing analysis by FTIR spectroscopy. *Proceedings of the Institution of Civil Engineers - Construction Materials* **2015**, *168* (5), 219−231.
(97) Helms, J. Spectroscopic Characterization of Dissolved Organic Matter: Insights into Composition, Photochemical Transformation and Carbon Cycling, 2012.
(98) Olsson, A.-M.; Salmén, L. The association of water to cellulose and hemicellulose in paper examined by FTIR spectroscopy. *Carbohydr. Res.* **2004**, *339* (4), 813−818.
(99) Tatsumoto, K.; Baker, J. O.; Tucker, M. P.; Oh, K. K.; Mohagheghi, A.; Grohmann, K.; Himmel, M. E. Digestion of Pretreated Aspen Substrates - Hydrolysis Rates and Adsorptive Loss of Cellulase Enzymes. *Appl. Biochem. Biotechnol.* **1988**, *18*, 159−174.
(100) Yang, B.; Wyman, C. E. BSA treatment to enhance enzymatic hydrolysis of cellulose in lignin containing substrates. *Biotechnol. Bioeng.* **2006**, *94* (4), 611−7.
(101) Klein-Marcuschamer, D.; Oleskowicz-Popiel, P.; Simmons, B. A.; Blanch, H. W. The challenge of enzyme cost in the production of lignocellulosic biofuels. *Biotechnol. Bioeng.* **2012**, *109* (4), 1083−1087.
(102) Ishizawa, C. I.; Jeoh, T.; Adney, W. S.; Himmel, M. E.; Johnson, D. K.; Davis, M. F. Can delignification decrease cellulose digestibility in acid pretreated corn stover? *Cellulose* **2009**, *16* (4), 677−686.
(103) Li, J. B.; Henriksson, G.; Gellerstedt, G. Lignin depolymerization/repolymerization and its critical role for delignification of aspen wood by steam explosion. *Bioresour. Technol.* **2007**, *98* (16), 3061−3068.
(104) Pu, Y. Q.; Hu, F.; Huang, F.; Davison, B. H.; Ragauskas, A. J. Assessing the molecular structure basis for biomass recalcitrance during dilute acid and hydrothermal pretreatments. *Biotechnol Biofuels* **2013**, *6*, 15.
(105) Sturgeon, M. R.; Kim, S.; Lawrence, K.; Paton, R. S.; Chmely, S. C.; Nimlos, M.; Foust, T. D.; Beckham, G. T. A Mechanistic Investigation of Acid-Catalyzed Cleavage of Aryl-Ether Linkages: Implications for Lignin Depolymerization in Acidic Environments. *ACS Sustainable Chem. Eng.* **2014**, *2* (3), 472−485.
(106) Kobayashi, T.; Kohn, B.; Holmes, L.; Faulkner, R.; Davis, M.; Maciel, G. E. Molecular-Level Consequences of Biomass Pretreatment by Dilute Sulfuric Acid at Various Temperatures. *Energy Fuels* **2011**, *25* (4), 1790−1797.
(107) Shuai, L.; Amiri, M. T.; Questell-Santiago, Y. M.; Heroguel, F.; Li, Y. D.; Kim, H.; Meilan, R.; Chapple, C.; Ralph, J.; Luterbacher, J. S. Formaldehyde stabilization facilitates lignin monomer production during biomass depolymerization. *Science* **2016**, *354* (6310), 329−333.

DOI: 10.1021/jacs.8b10242
J. Am. Chem. Soc. 2019, 141, 12545−12557